The molecular and cellular anatomy of a fetal programming defect – the impact of low protein diet on the developing kidney.

Kieran M. Short[a1], Giovane G. Tortelote[b1], Lynelle K. Jones[a], Fabiola Diniz[b], Francesca Edgington-Giordano[b], Luise A. Cullen-McEwen[c], Jan Schröder[d,e], Ashley Spencer[a], Andrew Keniry[f,g], Jose M. Polo[d,e], John F. Bertram[c], Marnie E. Blewitt[f,g] , Ian M. Smyth[a*], Samir S. El-Dahr[b*].

Affiliation list:

a. Kidney Development and Disease Laboratory, Department of Anatomy and Developmental Biology, Development and Stem Cells Program, Monash Biomedicine Discovery Institute, Monash University, Australia.
b. Section of Pediatric Nephrology, Department of Pediatrics, Tulane University School of Medicine, New Orleans, Louisiana, USA
c. Kidney Development, Programming and Disease Laboratory, Department of Anatomy and Developmental Biology, Development and Stem Cells Program, Monash Biomedicine Discovery Institute, Monash University.
d. Department of Anatomy & Developmental Biology, Monash University, Melbourne, Victoria, Australia.
e. The Australian Regenerative Medicine Institute, Monash University, Melbourne, Victoria, Australia.
f. The Epigenetics and Development Division, WEHI, Parkville, VIC, Australia.
g. The Department of Medical Biology, The University of Melbourne, Parkville, VIC, Australia.

* Co-corresponding authors.
[1] Co first authors.

Prof Ian Smyth
Kidney Development and Disease Laboratory
Department of Anatomy and Developmental Biology
Development and Stem Cells Program
Monash Biomedicine Discovery Institute
19 Innovation Walk
Monash University
Melbourne, Australia 3800
Ph: +61 (0)3 99029119
Email: ian.smyth@monash.edu

Prof Samir El-Dahr
Pediatric Nephrology,
Department of Pediatrics,
Tulane University School of Medicine,
1430 Tulane Avenue,
Tulane, New Orleans, LA 70112
Ph: +1 504-988-6692Email: seldahr@tulane.edu

Competing Interest Statement: No competing interests to disclose.

Abstract

Low nephron number correlates with the development of hypertension and chronic kidney disease later in life. While intrauterine growth restriction caused by maternal low protein diet (LPD) is thought to be a significant cause of reduced nephron endowment in impoverished communities, its influence on the cellular and molecular processes which drive nephron formation are poorly understood. We conducted a comprehensive characterization of the impact of LPD on kidney development using tomographic and confocal imaging to quantify changes in branching morphogenesis and the cellular and morphological features of nephrogenic niches across development. These analyses were paired with single-cell RNA sequencing to dissect the transcriptional changes that LPD imposes during renal development. Differences in the expression of genes involved in metabolism were identified in most cell types we analyzed, yielding imbalances and shifts in cellular energy production. We further demonstrate that LPD impedes branching morphogenesis and significantly reduces the number of pretubular aggregates – the initial precursors to nephron formation. The most striking observation was that LPD changes the developmental trajectory of nephron progenitor cells, driving the formation of a partially committed cell population which likely reflects a failure of cells to commit to nephron formation and which ultimately reduces endowment. This unique profile of a fetal programming defect demonstrates that low nephron endowment arises from the pleiotropic impact of changes in branching morphogenesis and nephron progenitor cell commitment, the latter of which highlights a critical role for nutrition in regulating the cell fate decisions underpinning nephron endowment.

Significance Statement

While a mother's diet and behavior can negatively impact the number of nephrons in the kidneys of her offspring, the root cellular and molecular drivers of these deficits have not been rigorously explored. In this study we use advanced imaging and gene expression analysis in mouse models to define how a maternal low protein diet, analogous to that of impoverished communities, results in reduced nephron endowment. We find that low protein diet has pleiotropic effects on metabolism and the normal programs of gene expression. These profoundly impact the process of branching morphogenesis necessary to establish niches for nephron generation and change cell behaviors which regulate how and when nephron progenitor cells commit to differentiation.

Introduction

Nephron endowment has a direct impact on renal function and is inversely related to the risk of hypertension and adult kidney disease (Poladia, Kish et al. 2006, Luyckx and Brenner 2010, Luyckx, Shukha and Brenner 2011). Endowment can vary 13-fold in normal human populations (Bertram, Douglas-Denton et al. 2011) but the intrinsic drivers of these differences are not fully known. While genetic factors no doubt account for some of this variation (different mouse strains have different endowment (Murawski, Maina and Gupta 2010), maternal disease and diet during pregnancy are also likely to significantly influence this measure as all nephrons in humans (and most in mice) are formed *in utero*. One such dietary variable is protein deficiency, which has been identified as a common global nutritional deficit (de Onis, Monteiro et al. 1993, Ghosh, Suri and Uauy 2012, Semba 2016) and one that has been exacerbated by the recent COVID-19 pandemic (Kakaei, Nourmoradi et al. 2022). However, the precise molecular mechanism by which maternal low protein diet (LPD) affects embryo and kidney development remains unclear.

Studies in rodent models have shown that an iso-caloric LPD leads to impaired kidney development and reduced nephron endowment, particularly in individuals with low birth weight (Langley-Evans, Welham and Jackson 1999, Hoppe, Evans et al. 2007) and that it predisposes to the development of hypertension and kidney disease in adult animals (Zeman 1968, Merlet-Benichou, Gilbert et al. 1994, Woods, Ingelfinger et al. 2001, Brawley, Itoh et al. 2003, Woods, Weeks and Rasch 2004, Goyal and Longo 2013). These observations indicate that appropriate quantities of high-quality protein during pregnancy are essential to offset imbalances causative of hypertension and chronic kidney disease later in life (Woods, Ingelfinger et al. 2001, Woods, Weeks and Rasch 2004). Therefore, a mechanistic understanding of how genetic and epigenetic changes influence nephron endowment in this context is of clinical importance.

Here, we set out to establish at a cellular and molecular level, across developmental time, the mechanisms by which a gestational low-protein diet (LPD) results in reduced nephron endowment. We show that LPD affects nephron number through a reduction in cell proliferation earlier in development along with alterations in the nephrogenic and branching morphogenesis programs. This in part results in a reduction in the number of nascent nephron structures (pretubular aggregates and renal vesicles). Single-cell sequencing of LPD kidneys indicates disruption to the cell metabolism, branching morphogenesis and nephrogenic differentiation transcription programs. Together, this study represents a fundamental advance in our understanding of the cellular and morphological disruption underpinning maternally influenced nephron deficit.

Results

Maternal LPD reduces postnatal body mass and nephron number.

To investigate the impact of LPD on fetal kidney development, male and female mice were fed modified chow for two weeks before conception, throughout pregnancy and until weaning. At embryonic day (E)14.5, body mass was similar between diets and placental mass was reduced by ~7% (SI Appendix, Fig. S1 and Data S1). At birth and postnatal day (P)21 body mass in LPD offspring was also lower than normal protein controls (9.5% and 16% respectively, Fig. 1A-C). Both newborn (Fig. 1D) and 3-week-old LPD mice (Fig. 1E) exhibited 19% and 23% fewer nephrons respectively (SI. Appendix, Data S1) confirming that the protein-deficient (but isocaloric) diet used in this study causes persistent low nephron endowment and intra-uterine growth restriction. No sex difference in body mass or nephron number were observed.

Maternal LPD alters embryonic kidney branching morphogenesis and nephrogenic niche number.

Given the importance of the reciprocal inductive signals between ureteric bud (UB) and nephron progenitor cells (NPCs) during kidney development, we wondered whether branching morphogenesis was affected by LPD and whether such changes contribute to reduced nephron endowment. Branching morphogenesis was assessed at E14.5 using Optical Projection Tomography (Short, Hodson and Smyth 2010) and at P0 by the number of peripheral SIX2 positively stained nephrogenic niches as a measure of the extent of branching (Short, Hodson and Smyth 2013). While a small 9% difference in niche number at P0 was identified (Fig. 2A), at E14.5 the tip number was invariant (Fig. 2B, SI. Appendix, Data S1). However, the same LPD embryonic kidneys had a 25% reduction in volume (Fig. 2C) and 18.4% reduction in surface area (Fig. 2D). This leads to an increase in ureteric tip density of approximately 16% in the E14.5 LPD kidneys (Fig. 2E). Notably, the terminal branch generations in the LPD offspring were significantly reduced in length, with the tips reduced by 22.2% and their "parents" by 15% (Fig. 2F). To determine if these changes altered the morphology of the ureteric tree, we compared our data with previously defined models of kidney branch patterning (Lefevre, Short et al. 2017). Branching is a dynamic process, and neighboring end branches and their tips normally fall in one of three local patterns based on the how the tips are inherited from parental branches (Lefevre, Short et al. 2017). Most branching patterning exhibits a mild asymmetry (Half Delay), and other more asymmetrical (Fibonacci) or perfectly symmetrical (Perfect, as in a simple bifurcation) patterns are noted. In the LPD kidneys, there are a greater number of highly imbalanced 'Fibonacci' patterned terminal branches (Fig. 2F). Similar increases in this pattern have been identified in kidneys with increased tip packing at the organ periphery (Lefevre, Short et al. 2017). On this basis, we assessed nearest-neighbor distances between tips and found this to be ~25% less in LPD offspring (Fig. 2G), analogous to patterning defects in *Spry1* mutant mice which also have decreased organ size but no change in branching (Lefevre, Short et al. 2017). These defects in ureteric branching, growth, patterning and tip packing may influence (or be influenced by) nephron formation.

Maternal LPD reduces progenitor cell proliferation and commitment to nephron formation.

The differences in branching and kidney size observed in LPD embryos prompted us to investigate whether proliferation of the ureteric and nephron progenitor cells was affected. A deficit in proliferative capacity would have a negative impact on branching and nephron differentiation. We imaged and counted markers for nephron progenitor cells (SIX2), ureteric bud (TROP2), and cell proliferation (PHH3) in wholemount-stained kidneys. At E14.5 following LDP exposure, nephrogenic niches showed a reduction in proliferation in both the ureteric tip epithelium (25.57%) and cap mesenchyme (27.44%) when normalized to the number of cells in the respective compartments (Fig. 3A-C). At P0, proliferation in the LPD cap mesenchyme was further reduced (37.5%) but UB proliferation had normalized (Fig. 3A-B, SI. Appendix, Data S1). By P2, no differences in UB/cap mesenchyme cell proliferation were noted (Fig. 3A-B). To determine the impact of LPD on nephrogenesis, we quantified the number of developing nascent nephrons at E14.5, P0 and P2 using the same markers scoring for pretubular aggregates (PTA), renal vesicles (RV), comma-shaped bodies (CSB), S-shaped bodies (SSB) and Stage IV (nearly mature) nephrons. Despite the preservation of nephrogenic tip niches at E14.5, LPD caused a consistent reduction in PTA number (60.2%, 37.3% and 41% respectively) and the total number of nephrons at any stage of differentiation (31.9%, 18.8% and 27.3% respectively) (Fig. 3C-D). The number of distally connected nephric segments indicated no differences *in utero*, but by P2 there was a 16.7% reduction in these structures (Fig. 3E). These results suggested that LPD affects the ability of NPC cells to commit to nephron formation.

Single-cell sequencing reveals developmental and morphological effects of maternal LPD.

To better understand the molecular mechanisms underlying these phenotypes, we assessed E14.5 and P0 kidneys by single-cell and single-nuclear RNA sequencing. Quality controlled, filtered and clustered datasets were assigned to different cell types using *a priori* known markers

(Fig. 4A-D). Diet did not induce an overt change in clustering cell content or UMAP structure (SI Appendix, Fig. S2) and as expected, the P0 kidney cells showed more differentiated cellular identities and lower proportions of undifferentiated cell types compared to the E14.5 kidney cells (Fig. 4D). A large proportion of the most variably expressed genes relate to age and are therefore common between the two diets (2968 and 2546 genes at E14.5 and P0 respectively), however dietary treatment altered 1032 and 1454 genes at these timepoints. Preliminary characterization of differential gene expression using gene ontology analysis revealed most changes in these clusters are related to developmental, morphological and metabolic processes (Fig. 4F and SI Appendix, Table S1 and S2) and that the nephrogenic and the ureteric bud lineages were those most impacted by LPD.

Maternal LPD impairs the differentiation of nephron progenitor cells and alters the expression of developmental and metabolic genes.

To understand how nephrogenesis was impacted by LPD, we first focused on the continuum of differentiating nephrons by sub-clustering the NPCs, committing NPCs, renal vesicle cells, S-shaped body cells and podocytes (Fig. 5A). Pseudotime was then inferred using Slingshot (Street, Risso et al. 2018) (Fig. 5B), and an unsupervised approach was used which did not pre-establish the direction or order of the assigned pseudotime values of cells. Supporting the application of pseudotime for this lineage, we found the resulting positioning of cells across pseudotime (when split by cluster labels) recapitulated the biologically established ordering of nephrogenic cell types (Fig. 5C). The inferred trajectory did not diverge between the diets (Fig. 5B), but the comparative distribution of cells across the lineage was uneven (Fig. 5D) with a greater number of LPD cells near the beginning of developmental pseudotime which includes mostly NPCs and committing NPCs (Fig. 5C-D, shaded area).

To explore the dynamic changes in gene expression between diets with a non-diverging pseudotime trajectory, we used tradeSeq (Van den Berge, Roux de Bezieux et al. 2020). The model generated by tradeSeq enabled the clustering of genes on a per-cell basis based on a weighted gene expression correlation, thereby enabling the grouping of genes whose expression values vary together over pseudotime (Fig 5E). This facilitates the identification of gene association patterns among different diets and the grouping of them into gene clusters (Fig. 5E, SI Appendix, Fig. S3). At E14.5, differentially expressed genes were associated with cellular metabolism, cell shape, cell-cycle, and differentiation (Clusters 1, 7 and 8, Fig. 5E, for full lists of genes by cluster and GO terms, see SI. Appendix, Data S2). In addition, genes having roles in signaling pathways activated during nephron induction and differentiation, such as HNF, NOTCH, and WNT signaling pathways were also affected by LPD (Clusters 2-6, Fig. 5E). Similarly, in P0 LPD NPCs, *Wnt* genes and genes required for renal vesicle morphogenesis were downregulated, such as *Six2*, *Cited1*, *Lhx1*, *Jag1*, *Pax2*, *Pax8* and *Bmp4* (Clusters 2 and 3, Fig. 5E). Given the importance of WNT signaling as an inductive factor of nephrogenesis, we further investigated the changes in expression of several WNT pathway genes over pseudotime and across diet identifying LPD-induced reductions in WNT signaling at both developmental stages (Fig. 5F). Staining for WNT4 protein, an important inducer of nephrogenesis, detailed modest reductions in LPD kidneys at E14.5 and significant deficits at P0 (Fig. 5G).

Cumulative altered cellular processes cause a failure in the progression of nephron progenitors to different cellular states in LPD offspring.

With many of the differentially expressed genes associated with early commitment and renal vesicle formation, we next focused on the cells associated with these processes – the naïve and committing nephron progenitor cells. The methods we used to analyze these cells employed both cluster gene expression analysis as well as pseudotime analysis approaches.

Beginning with the naïve NPCs, the UMAP projections of the subclustered NPCs revealed areas of diet specific cell enrichment on the UMAP_1/UMAP_2 projection at P0 and E14.5 (Fig. 6A-B, SI Appendix, Fig. S4A-B). When comparing gene expression within the cluster, at E14.5 we observed downregulation of several genes in LPD kidneys, associated with cell cycle and proliferation such as: *Ybx3*, *Ptn*, *Gpc3* and *Rcc2* (Table 1), which corroborates the decreased NPC proliferation observations (Fig. 3B). GO analysis returned terms associated with cell proliferation involved in metanephric development (GO:0072203; FDR 0.008), indicating that the LPD affects both maintenance of the progenitor pool and their continued role in development (see SI Appendix, Data S2 and Table S2 for complete GO analysis results). Within the P0 NPC cluster, LPD induced downregulation of several genes including *Dach1* (Table 1) which interacts with *Eya1* in the nascent nephrons (Ayres, Shum et al. 2001, Ikeda, Watanabe et al. 2002) and *Pdgfc,* expressed in nephron progenitor cells that are in contact with the ureteric tip at E11.5 (Ding, Wu et al. 2000, Wu, Liu and Ding 2018) (Table 1). *Pdgfc* and *Eya1* are both critical to the establishment, maintenance and differentiation of NPCs (Li, Ponten et al. 2000, Sajithlal, Zou et al. 2005). This data indicates that reciprocal inductive signals present during kidney development were also affected by the LPD which may reflect the branching phenotype observed (Fig. 2F).

To assess the transition of cells from a naïve state towards a committed state, we used pseudotime analysis to reveal pools of LPD cells gathered at the ends of pseudotime at both ages (Fig 6C-E) with the distributions being quantifiably different ($D = 0.443$, $p < 2.2e-16$ at E14.5, and $D = 0.386$, $p < 2.2e-16$ at P0, KS test). At E14.5, the naïve NPCs from the LPD cohort occupied a pseudotime bracket almost devoid of NPD cells (Fig. 6E), and to a lesser degree at P0 (Fig. 6F). The difference in gene expression between this LPD pool and the NPD nephron progenitors is primarily the expression (and lack of expression) of several cell commitment genes SI Appendix, Fig. S4 C-D and Table 1) for example, *Cited1* (-0.28Log2FC) relative to *Crym* (0.99 Log2FC). This change is unexpected because the upregulation of *Crym* and relatively unchanged *Cited1* in this pseudotime-advanced specific LPD pool of NPCs suggested that they were in a more “advanced” differentiation state. However, the cells expressed naïve NPC markers and commitment genes were mostly absent (only a small number of cells expressed *Wnt4* and *Itga8*, and at low levels) (SI Appendix, Fig. S4D). In general, the remaining gene expression changes across NPC pseudotime fall broadly into several groups (Fig 6G-H). At E14, LPD NPCs exhibited downregulation of genes involved with NPC fate determination pathways such as WNT, AKT and HOX as well as upregulation of WNT and AKT inhibitors (Fig. 6G, SI Appendix, Data S2). At P0, several genes were downregulated in LPD kidneys that are related to epithelialization and renal vesicle formation (*Magi2*, *Pax2*, *Itga8*, *Itga9*, *Pbx1* and *Shroom3*) (Fig. 6H, SI Appendix Table S1). Taken together these pseudotime analyses indicate gene expression changes in nephron progenitors in LPD kidneys was consistent with the morphological alterations observed, including a reduced cell proliferation (Fig. 3B) and eventual PTA differentiation in the progenitor niche.

LPD promotes abnormal pseudotemporal progression of committed nephron progenitor cells.

To form pretubular aggregates, NPCs must enter the committing NPC stage. Given the reduction in pretubular aggregates in the LPD kidneys, we next sought to understand whether the changes in the NPCs correlating with differences in developmental progression were resolved once cells reached the committed NPC stage. To this end, the committing nephron progenitors were subclustered (Fig. 7A-B) which revealed that like their “parents”, LPD cells separated from the NPD cells. At E14.5, GO terms related to kidney development and tubule morphogenesis (a renal vesicle forming process) were present, with genes such as *Crym* mis-expressed (Table 2 and SI Appendix, Data S2). The upregulation of *Crym* expression just before epithelization suggests a continued compromised transition to pretubular aggregates cells and epithelialized renal vesicles. At P0, several genes associated with nephron progenitor identity were downregulated in LPD kidneys such as *Pax2*, *Bmper*, *Wt1*, and *Magi2* (Table 2, Fig7J), giving support for the reduction in PTAs in the LPD kidneys (Fig. 3C). Genes associated with regulation of RNA metabolism and

splicing were upregulated in the P0 committing nephron progenitors in LPD kidneys. In addition, differential expression identified genes related to nuclear division, nuclear chromosome segregation and mitosis (*Rcc2*, *Cdk2ap1*, *Ccnd1* and *Hnrnpa*) at E14.5 indicating a continued metabolic effect in these cells after transitioning from a naïve nephron progenitor state.

Interestingly there were common effects of LPD on both the naïve nephron progenitors and the committing nephron progenitors over pseudotime. These include significant changes in the distribution of cells across pseudotime ($D = 0.136$, $p = 1.502e-11$ at E14, $D = 0.265$, $p < 2.2e-16$ at P0, Two-sample KS test) with the committing NPCs also higher in abundance at the beginning of pseudotime (Fig. 7C-D). Furthermore, among the many changes (Fig. 7E-F, SI Appendix Data S2), downregulation of *Wnt4*, *Fgf8* and *Bmp7* was present, sharing a similar effect to the naïve NPCs. Entry into, and exit, from the committed state requires the differentiation signals of these genes (for a review see (O'Brien 2019)) which are downregulated over pseudotime in both types of LPD NPCs (SI Appendix, Fig. S6). This may be the reason why in LPD kidneys, naïve NPCs are concentrated at the end of pseudotime and the committed NPCs are concentrated at the beginning of pseudotime (at both E14.5 and P0).

The branching and proliferation phenotype in the ureteric epithelium have underlying deficits in proliferative and developmental pathways.

Given that the proliferation in ureteric tip cells was reduced (mirroring the NPC proliferation), as were the lengths of the ureteric tips and trunks (Fig. 2) in LPD kidneys, we next investigated the UB-tip and UB-trunk cell populations at a single cell level (Fig. 8A-B). At the level of cell type, reduced expression of markers of cell proliferation and mitosis were observed at E14.5 (*Hnmpa0*, *Ybx3*, *Rcc2*, *Gpc3*, *Cdk2ap1*, see Table 3) which is consistent with their reduced proliferation. We also identified upregulation of *Glo1* and *Aldh1a3* which are linked to metabolic stress and associated alterations in cell proliferation (Luo, Dallaglio et al. 2012, Kim, Jung et al. 2022). While there were only minor differences in the distributions across pseudotime ($D = 0.14379$, p-value $< 2.2e-16$ at E14.5, and $D = 0.086943$, p-value $= 0.0003057$ at P0, KS test) (Fig 8. C-D), assessment of gene expression in the ureteric clusters and across pseudotime trajectories revealed impacts on metabolic, cell cycle, developmental, and *Wnt* genes (Fig. 8E-F). These differences were associated with cell proliferation (*Hdac9*, *Erbb4*, *Fgf12*), cytoskeleton remodeling and cell adhesion (*Shroom3*, *Tenm2*, *Ctnnd2*, *Robo1*, *Nrg3*). *Shroom3* and *Errb4* play important roles in the differentiation of ureteric trunk cells by influencing cellular remodeling and duct cell mis-polarization (Nishimura and Takeichi 2008, Veikkolainen, Naillat et al. 2012) . Notably, at P0, *Wnt9b* expression is lower in LPD kidneys across pseudotime, with the greatest difference toward the trunk end of pseudotime (Fig. 8F), where *Wnt9b* is normally expressed and is required for *Wnt4* expression (Carroll, Park et al. 2005). While immunofluorescent staining did not reveal any major changes in WNT9B levels (SI Appendix, Fig. S5), *Wnt9b* heterozygote mice exhibit a weak induction of WNT4 (Carroll, Park et al. 2005) which is consistent with the changes in the NPC lineages in the LPD kidneys in the present study.

LPD causes a disrupted metabolism gene expression profile throughout the kidney.

Unifying the impact of the dietary intervention on the cellular metabolism of the developing kidney, we initially saw a consistent disruption in several metabolic pathways in all cells and both ages in response to LPD. While some of the metabolic genes that are differentially expressed in LPD differ between the two ages and cell types within the same kidney, many genes were associated with the same or similar pathways as defined by intersecting GO ontology terms (see SI. Appendix, Data S2). The pathways broadly included ATP production, RNA metabolism, and metabolic stress. The genes associated with ATP metabolism included *Atp1a1*, *Atp5c1*, *Cpt1a*,

Gapdh and *Trp53*. *Trp53* (*p53*) is downregulated in all 18 clusters at E14.5 and plays an important role in the NPC renewal and commitment process (Li, Liu et al. 2015). Upon genetic deletion of *Trp53* (Li, Liu et al. 2015), the most transcriptionally affected gene in NPC cells is *Pck1*. *Pck1*, a dietary responsive gluconeogenesis gene (McGrane, de Vente et al. 1988) is also downregulated in the nephrogenic lineages at both E14.5 and P0 (SI. Appendix, Data S2).

RNA metabolic processes were also affected by LPD, including genes associated with the regulation of amino acid levels, transcription of ribosomal proteins and translation. Prominent examples included the downregulation of *Hnrnpa0* and *Ybx3* which are involved in the regulation of RNA and amino acid levels (for a review of Hnrnp see (Thibault, Ganesan et al. 2021), (Cooke, Schwarzl et al. 2019)) (Table I and SI. Appendix, Data S2). Alterations in the transcription of ribosomal protein-coding genes (many of the *Rps/l* family genes) were also detected at both ages, which are indicative of a general impact on transcriptional and translational processes caused by LPD.

Metabolic stress gene expression changes in the embryonic and postnatal kidneys induced by LPD at E14 and P0 as shown in Table I and Supp. Appendix, Table S1. We found upregulation of *Glo1*, *Ldhb*, *Dera* and *Rdh10* as well as Ap-1 factors like *Fosb* and *Jun* and the transcription factor *Atf4*. ATF4 is known for its role in regulating the expression of genes involved in oxidative stress, amino acid (and protein) synthesis, and cell differentiation (Torrence, MacArthur et al. 2021) which all may contribute to the proliferation and differentiation deficits observed in the LPD kidneys.

Discussion

Nephron deficit is one of the principal features of intrauterine growth restriction caused by maternal malnutrition. We have used a model of dietary intervention which reduces protein intake (while maintaining caloric balance) to induce an ~25% reduction in nephron number at birth. We have used this model to explore both the cellular and molecular bases for reduced nephron endowment. Cellular metabolism generates the necessary energy, amino acid balance, transcriptional and translational platform for development in all organisms (Diaz-Cuadros, Miettinen et al. 2023), and the LPD diet induced many changes in metabolism gene regulation in almost every kidney cell type analyzed. We found metabolic stress, RNA metabolism and ATP production genes downregulated throughout the kidney and in the nephrogenic lineage. This is important because the downregulation of genes involved with energy production are known to play direct roles in NPC commitment (Liu, Edgington-Giordano et al. 2017) and nephron number (Chevalier 2020).

Branching morphogenesis of the ureteric epithelium and maintenance and commitment of nephron progenitor cells are co-dependent processes which are instrumental in establishing nephron endowment (Carroll, Park et al. 2005, Short, Combes et al. 2014, Short, Combes et al. 2018). In the branching ureteric epithelium, we find that despite maternal LPD reducing kidney size and decreasing cellular proliferation, it does not impact upon the branching program itself. Instead, kidneys at mid-gestation have shorter branches and a higher tip density which leads to patterning defects. Notably, metabolic demands are a limiting factor in driving cell proliferation during ureteric epithelial morphogenesis (Fernandes-Silva, Alves et al. 2021) and likely play a role in regulating the abnormalities in UB development we observed. In the nephrogenic niche, we find that LPD leads to a striking reduction in the commitment of progenitor cells to pretubular aggregates and, consequently, to more mature nephrogenic structures. Interestingly, the number of mature “connected” nephrons does not change during embryonic development, suggesting that the first round of nephron formation is unaffected by LPD, however the ~50% reduction in PTAs during later development underpins impaired nephron formation reflected in the number of mature nephrons that differentiate (and integrate) at or around birth. These observations suggest that

LPD kidneys experience an ongoing and persistent defect in the differentiation of nephron progenitor cells.

The shortening of the ureteric trunk and outer branch generations observed in LPD kidneys correlates with altered expression of several cell cycle genes including upregulation of *Bgt2* (a cell cycle repressor (Sima, Zhang et al. 2016)) and reductions in *Shroom3* and *Errb4* in the ureteric trunk cells that affect cellular remodeling and duct cell mis-polarization (Nishimura and Takeichi 2008, Veikkolainen, Naillat et al. 2012). While most of the RET pathway genes that control UB branching and growth were unaffected, *Gdnf* and the Gdnf co-receptor *Gfra1* were downregulated in LPD at E14.5, as were branching induction genes expressed elsewhere in the kidney (*Dach1* (Ayres, Shum et al. 2001, Ikeda, Watanabe et al. 2002), and *Ptn* (Sakurai, Bush and Nigam 2001)). As epithelial cells transition and differentiate from the UB-tip through to the collecting duct, they transiently express several genes which are central to the induction of nephrons from naive precursor cells. We used pseudotime analysis to recapitulate the UB maturation process (Fig 8D) and identified a reduction in *Wnt9b* as cells progress along this pathway (Fig. 8F). This is significant because deletion of *Wnt9b* alters cell movement and polarity within the ureteric trunk (Karner, Chirumamilla et al. 2009). In addition it acts as a paracrine signal that regulates the differentiation of adjacent primed nephron progenitor cells (Karner, Das et al. 2011) and also induces expression of *Wnt4* in the committing nephron progenitors, pretubular aggregates and renal vesicles (Carroll, Park et al. 2005). *Wnt4* then acts in an autocrine and paracrine manner to induce its own expression (Kispert, Vainio and McMahon 1998). We find widespread evidence for deficiencies in this pathway in LPD kidneys, including reduced *Wnt4* expression in advanced pretubular aggregate/renal vesicles), and accumulation of PTA's, whose further differentiation is contingent on normal WNT signaling.

When considering the differentiation program of NPCs by pseudotime analysis we found significant impact on WNT, NOTCH and AKT pathways with genes such as *Lrp5*, *-6*, *Axin2*, *Dvl1*, *Wnt4*, *Notch2* reduced at E14.5 and P0 between NPC and podocyte stages. We also identified irregularities in WNT pathway gene expression in the LPD NPCs at E14.5 including reduced expression of metanephric development and RV formation genes. These changes mirror the reductions in *Wnt9b* expression in the developing UB-tip/trunk affecting the genesis of renal vesicles. Taken together, we propose that these changes in developmental gene expression lead to the formation of a unique subpopulation of LPD-specific NPCs with mixed identity whose capacity to commit to nephron differentiation is either abrogated or prevented. These cells have an unusual gene expression signature, exhibiting increased *Wnt4*, *Crym*, and differentiation markers *Ybx3*, *Gpc3* and *Rcc2* (a metaphase cell cycle marker) - which are hallmarks of more differentiated NPCs. However, at the same time they co-expressed markers of uncommitted cells such as *Cited1*. Notably in the whole-kidney clustering, they grouped with other NPCs while the committed LPD and NPD NPCs clustered separately. This contradictory gene expression state and differentiation profile indicates that these cells are at the point of differentiation but fail to make the transition to PTAs – an observation consistent with the deficit in these structures in embryos exposed to LPD. While a similar subset of cells was not apparent at P0, pseudotime analysis still profiled less differentiated LPD NPCs, even though proliferation was reduced, and total cell number was similar. The idea that such dietary interventions might lead to the formation of progenitors that are blocked from differentiation are supported by a recent paper by Guo et al. illustrating how levels of canonical WNT signaling regulate a delicate balance between self-renewal and differentiation in NPCs (Guo, Kim et al. 2021).

A recent study using LPD found a 28% reduction of nephrons at birth in Wistar rats (Sene, Scarano et al. 2021). MicroRNA (miRNA) sequencing was performed on embryonic day 17 embryos (similar to E15 in mice), along with immunostaining of suspected miRNA targets at the same age. While the reduction in nephron number and proliferation of LPD UB-tip and NPCs was similar to the E14.5 cohort in this study, the Sene study did not cover several important changes which this study addressed. Chiefly, the impact on growth and patterning on the UB-tip and

ureteric tree; the normalization of NPC and UB-tip proliferation at P2 and P0 respectively; or the pan-developmental impact on the transcriptional and morphological changes in nephron progenitor commitment and differentiation.

Another recent study using a calorie restricted diet (CRD) in mice (Makayes, Resnick et al. 2021) has shown in isolated NPCs and *in vitro*, an involvement with methionine metabolism and the MTOR pathway. While neither the process of nephrogenesis nor branching morphogenesis was assessed in the CRD study, other similarities and differences are apparent. Common to both is a reduction in body mass, postnatal nephron number and proliferation in NPCs at E14.5. However, at birth, no differences in NPC proliferation in CRD kidneys were apparent, unlike the LPD kidneys (where normalization only happens at P2 in the LPD). Also, this LPD study did not identify any changes in mTor expression in any LPD kidney clusters at either E14.5 or P0. The analysis of proliferation in both studies indicates a similar reduction in cell cycle early in kidney development, but proliferation returns to normal sooner in CPD NPCs than in LPD NPCs. This highlights the differences between the two nutritional challenges to kidney development.

Our findings present a comprehensive analysis of nephron deficit caused by intrauterine growth restriction brought about by a diminished commitment of nephrogenic precursor cells and reduced tip growth in branching morphogenesis, resulting in less nascent nephrons. The downregulation of differentiation and WNT pathway genes within clusters and across pseudotime is reflected in the reduced number of pretubular aggregates and nascent nephrons throughout development. These effects are underpinned by a reduction in cellular proliferation, highlighted by a reduction in cell cycle gene expression and energy production genes. The reduction in cellular metabolism genes and pathways is a prominent feature of all cell types and highlights the nutritional impact on the cell fate decisions that underpin this nephron deficit phenotype.

Materials and Methods

IACUC statement

All animal experiments in this study were assessed and approved by Monash University and the Tulane University Institutional Animal Care and Use Committee. Animal work was conducted under applicable laws governing the care and use of animals for scientific purposes. Animal Ethics Committees (MARP/18204).

Animals and diets

CD1 mice were acquired from Charles River Laboratories and C67BL6/J mice were sourced from Jax Laboratories via Monash University. Six-week-old females were fed either Normal (20-18%) protein diet (ENVIGO, cat# TD.91352, Specialty Feeds, cat# AIN-93G respectively) or Low (6-8%) protein diet (Specialty Feeds, cat# SF01-026, ENVIGO, cat# TD.90016) for 2 weeks. International transport restrictions between the El-Dahr and Smyth groups located in the USA and Australia respectively determined the differences between the diets. See SI. Appendix, Data S1 for diet composition. While there are differences and similarities between the diets and animal strains, the kidney phenotype presented in the present study is the same in the LPD exposed offspring.

Animal collection

Time mated pregnant females were euthanized at approximately E14.5, E19.5 (day of vaginal plug being E0.5), and pups euthanized at P0 and P2. Mouse embryos and pups were staged according to limb staging (Wanek, Muneoka et al. 1989), dissected and the kidneys were removed and either fixed in 4% formalin and put in ice-cold PBS, or liquid nitrogen (depending on experimental requirements).

Niche assessment

Dissected kidneys at E14.5, P0 and P2 were stained with antibodies to NPCs (SIX2, Proteintech cat#: 115621AP, 1:600 dilution), ureteric tree (TROP2, R&D Systems, cat#: AF1122, 1:20 dilution), proliferating nuclei (PHH3, Abcam, cat#: AB10543, 1:300 dilution) and nuclei (DAPI, Sigma, cat#: D9542, 1mg/mL dilution) with appropriate Alexa Fluor secondary antibodies (Life Technologies) as previously described (Combes, Short et al. 2014). The stained kidneys were cleared using BABB (Benzyl alcohol/Benzyl benzoate, 1:2, Sigma, cat numbers 108006 and B6630, consecutively) and imaged using a Leica SP8 confocal microscopy at 20X and quantified using Imaris (Oxford Instruments). In order to accurately sample the cellular state across the kidney, morphological assessments were made for per-tip and per-cap (i.e. per niche) with a minimum 6 tip/cap combinations per imaged field, with usually 6 fields per kidney covering both sides, as well as at least one pole (less fields were available at E14.5 where the kidneys are smaller). A grand total of 78 niches at E14.5 (from 8 kidneys), 564 at P0 (from 20 kidneys), and 289 at P2 (from 14 kidneys) were assessed. Cell numbers, proliferating cell numbers, cap-mesenchyme, and tip volumes were all measured for each niche, as well as an assessment of associated nephric structures. Nephric structure assessment was qualitatively performed by observation of nuclei in Z slices near ureteric tips, and defining aggregates, luminal balls of cells, or elongated tubular luminal structures of different lengths and morphologies. This enabled the

distinction between nephron progenitor cells, pretubular aggregates, renal vesicles, comma/S-shaped bodies, and nephrons.

Histological staining

Dissected kidneys at E14.5, P0 were fixed and histologically sectioned and were stained with antibodies to detect Wnt4 (anti-Wnt4, R&D systems, cat# AF475, dilution 1:100), Wnt9b (anti-Wnt9b, R&D Systems, cat# AF3669, 1:100 dilution), Six2 (as above but at 1:400 dilution) in different combinations. The primary markers were detected with secondary antibodies using HRP (Jackson Immuno Research, cat# 705-036-174, 1:100 dilution), Alexa Fluor 555 (Thermo Fisher, cat# A-31572, 1:400 dilution), fluorescent tagged Dolichos Biflorus Agglutinin (DBA) (Vector Labs, cat# FL1031, 1:100 dilution), and nuclei with Hoechst-33342 (Thermo Fisher, cat# 62249, dilution 1:10,000 dilution).

Optical Projection tomography, branching, and niche number analysis

TROP2 antibody stained E14.5 kidneys were mounted in agarose, cleared, and imaged in a Bioptonics OPT3001 instrument using 800 projections at 1024x1024 pixel resolution as previously described (Combes, Short et al. 2014). Tomography projections were reconstructed using nRecon (Bruker) and Tree Surveyor was used to map the ureteric tree as previously described (Short, Hodson and Smyth 2013, Combes, Short et al. 2014) which enabled the determination of branch lengths, surface area, kidney volume, tip number and tip to tip distances. Branch patterning was quantified from Tree Surveyor data using python scripts as previously described (Lefevre, Short et al. 2017). To count tip/niche number at P0, whole kidneys were stained with SIX2 antibody (1:600), and an appropriate Alexa-fluor secondary antibody (Life Technologies), cleared, and imaged using optical projection tomography as above. SIX2 positively stained clusters/niches were classified by their characteristic ('horseshoe') shape and manually counted in Imaris (Oxford Instruments). Each cluster represents a single niche, and by extension a single ureteric/collecting duct tip (Short, Combes et al. 2014).

Statistics

In order to statistically test the differences between diets where repeated measurements are taken per-kidney (e.g., proliferation or associated nephric structures per niche from confocal data, body mass over time, or branching measurements from OPT/Tree Surveyor), linear mixed-effects models were applied to the data within the R statistical environment using the stats or lme4 packages. The use of two factor ANOVA enabled the partitioning of inter-kidney variance within the treatment group. To quantify the cumulative probability of differential association of cells associated across pseudotime, we used a Two-sample KS (Kolmogorov-Smirnov) test. Two sample tests were performed using an unpaired two-tailed T-test.

Nephron counting

NPD and LPD offspring were collected at P0 to assess the impact of gestational LPD feeding on nephron number. Pups were weighed, sexed and kidneys dissected in PBS and fixed in methacarn (60% absolute methanol, 30% chloroform, and 10% glacial acetic acid). Following processing to paraffin, the kidneys were exhaustively sectioned at 4 µm. Ten evenly spaced section pairs were systematically sampled and stained with lectin peanut agglutinin (PNA; Sigma-Aldrich, Castle Hill, NSW, Australian; L3165) to identify the plasma membranes of podocytes. Following counterstaining with hematoxylin, section pairs were projected using a light microscope and all PNA+ structures (representing S-shaped body stage to capillary loop stage glomeruli)

were counted using the physical dissector/fractionator counting principle (Cullen-McEwen, Armitage et al. 2012). The same approach was applied at P21, except the section thickness was increased to 5 µm.

Single-cell and nuclear RNA-sequencing and data analysis

Two groups of kidneys five E14.5 kidneys, from 2 different females, per diet were pooled together and processed to obtain single-cell suspension as previously described (Combes, Phipson et al. 2019). For single nuclear sequencing at postnatal day 0, pairs of kidneys were snap frozen in liquid nitrogen immediately after dissection. Single nuclear approach was specifically chosen for the postnatal kidneys because they require significantly more physical and enzymatic intervention for cellular dissociation than E14.5 kidneys, and this treatment may significantly impact cellular and sequencing quality. Frozen nuclei were thawed in nuclei lysis buffer (Sigma) in a 15mL tissue grinder (Kimble), ground, and isolated by centrifugation and washing before being purified by flow cytometry, as per (Grubman, Chew et al. 2019). Approximately 10k cells or nuclei (per sample) were emulsified with Single Cell 3' V3 beads (10X Genomics) and libraries generated on a 10X Chromium instrument. Libraries were amplified and sequenced using an MGITech MGISEQ200RS with a target of 50k reads per cell. Raw sequencing data was processed using Cell Ranger (v5.0, 10X Genomics) and transcripts mapped to a reference genome based on mm10 (v3) with pre-mRNA (nuclear) optimizations. Single cell preparation and sequencing of E14.5 samples was performed using published embryonic kidney dissociation methods (Combes, Phipson et al. 2019) and using protocols from 10X Genomics. Single-cell samples were sequenced with an Illumina NextSeq 2000 mRNA (cellular), and processed as above, but with mapped to mm10 (v3) genome mRNA. All sequencing analysis was performed in R with the aid of the Tidyverse packages (Hadley Wickham 2019). Seurat (v3.2) (Hao, Hao et al. 2021) was the major package used to import and analyze the cell/nuclear sequencing data. Cells with no counts or less than 300 genes detected, or more than 15% of mitochondrial genes were removed. Cluster identity was determined using 4000 highly variable genes, and the first 20 principal components. We obtained lists of DE genes for each cluster using the Seurat FindAllMarkers function and upregulated genes in each cluster were used to classify the different cell types. To test differential gene expression between diets, Seurat objects were converted to single-cell experiment objects and the limma package (Ritchie, Phipson et al. 2015) was used for testing. To further understand gene biological functions and associated pathways, we performed the gene ontology (GO) and KEGG pathway enrichment analysis with Goanna (from limma), and additional unsupervised and supervised ontology analysis with STRING and DAVID (Huang, Sherman et al. 2007), and GOfuncR (Grote 2023) for extracting gene annotations from ontologies. Pseudotime analysis was performed using Slingshot (Street, Risso et al. 2018), and differential gene expression analysis across pseudotime was performed using TradeSeq (Van den Berge, Roux de Bezieux et al. 2020). The sequencing datasets used in this work are available on GEO accession ID GSE240044.

Acknowledgments

We would like to acknowledge the many contributors to this work including technical assistance from Grace Jackel and Guizhi Sun at Monash University. We also would like to thank James LeFevre (University of Queensland) and Alexander Combes (Monash University) for bioinformatic and data processing discussions. We thank staff and managers of the facilities used for this work, including Monash Animal Research Platform, Monash Micro Imaging, Monash FlowCore, Monash Micromon Genomics, Monash Histology Platform, the Monash Bioinformatics core, the Tulane Center for Translational Research in Infection & Inflammation NextGen Sequencing Core. This work was funded by Tulane School of Medicine Startup Grant to Dr. Tortelote, NIDDK R01 grant (5R01DK118231) to Prof. El-Dahr, and NHMRC project grant APP1080746 to Profs. Smyth, Bertram and Belwitt.

Figures and Tables

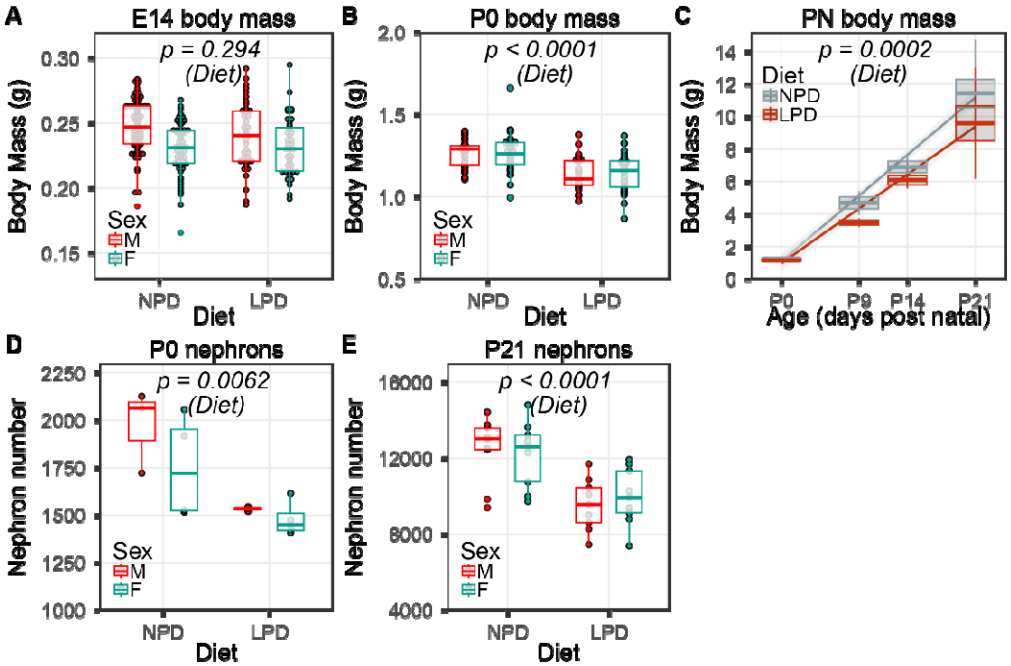

Figure 1.

Maternal low protein diet affects the mouse embryo and kidney. At embryonic day E14, body mass is no different depending on diet (A, n=133/86 NPD/LPD, $p = 0.294$), but this changes by birth (B, n = 66/56, $p < 0.0001$). Postnatally, a low protein diet continues to impact postnatal body mass through to PN21 (C, n=133/86 P0, n= 18/15 P9, n= 24/14 P14, n=59/41 P21, NPD/LPD, $p = 0.0002$). At birth, total nephron number is 19% lower in LPD than NPD (D, n=7/7, $p = 0.0062$) and by postnatal day 21, nephron number is 23% lower in LPD (E, n = 18/18, $p < 0.0001$). No sex differences in these parameters were found. Orders for sample numbers are NPD/LPD.

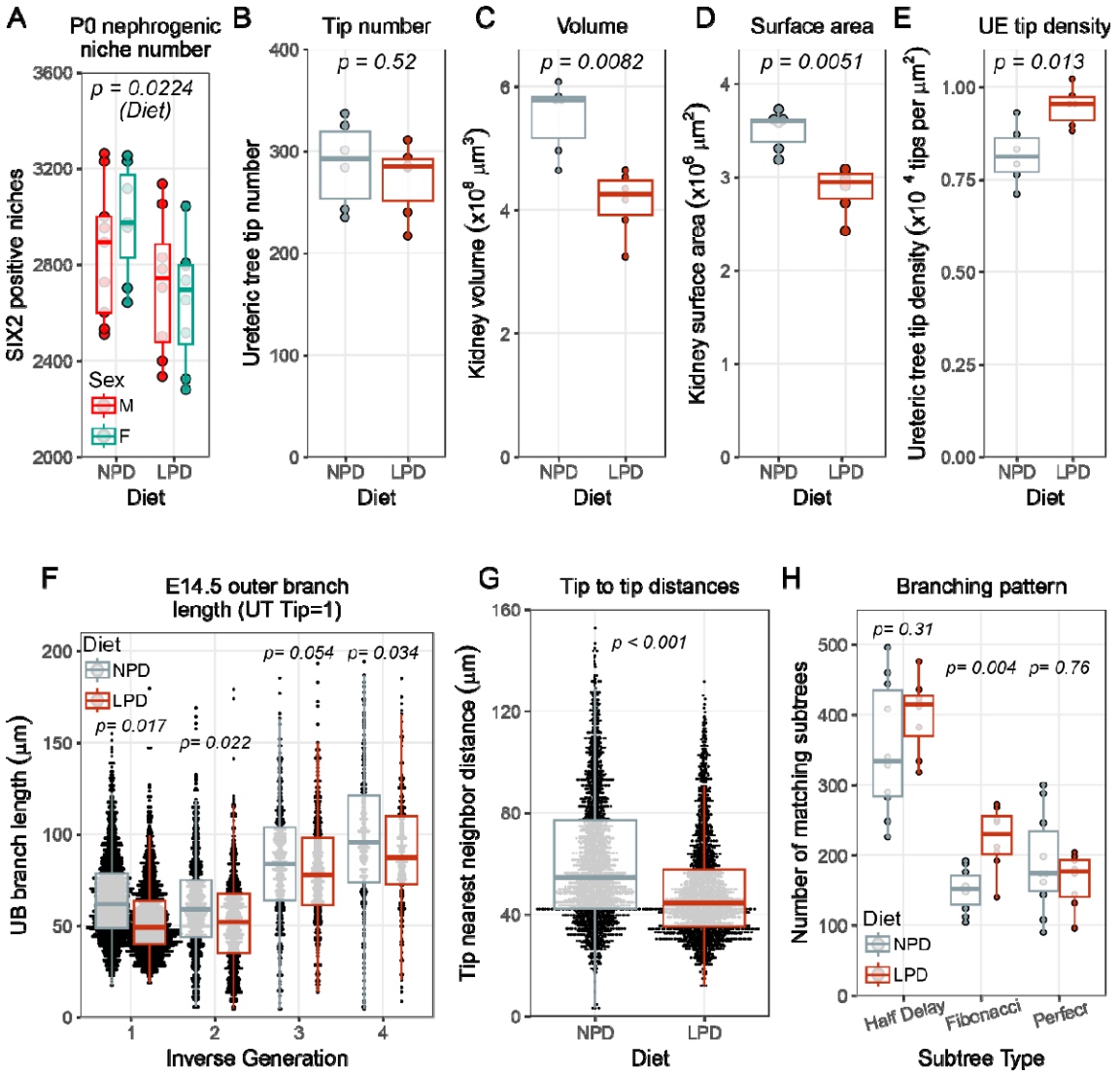

Figure 2.

The impact of LPD on branching morphogenesis and kidney growth. At the day of birth, the number of Six2 positive nephrogenic niches is lower in LPD pups and there are no differences between the sexes (A, n=16/16, *p = 0.0224* for diet). This represents a reduction in tip number of the ureteric tree. Although earlier at embryonic day E14.5, the tip number is unchanged (B, *p = 0.52*) but those tips are packed into a smaller kidney (C, *p = 0.0082*) with a smaller surface area (D, *p = 0.0051*) leading to a higher tip density (E, *p = 0.013*). The outer branches of the ureteric tree starting at the tips towards the ureter are consistently shorter in length in the LPD kidneys (F, tip *p = 0.012*, tip parent *p = 0.022*, tip great grandparent *p = 0.034*). The tip grandparent is *n.s*, The shorter branches which are packed more densely have shorter tip to tip distances (G, *p = 0.00072*) with less space to grow. This tighter packing partially affects the LPD branching pattern, with the branch patterns at the periphery fitting a Fibonacci tip state model (Lefevre, Short et al. 2017) at a greater proportion than the NPD kidneys (H, *p = 0.0044*). N = 6/6 NPD/LPD for whole kidney measurements, and branches analyzed per kidney are n > 1000. n.s., not significant.

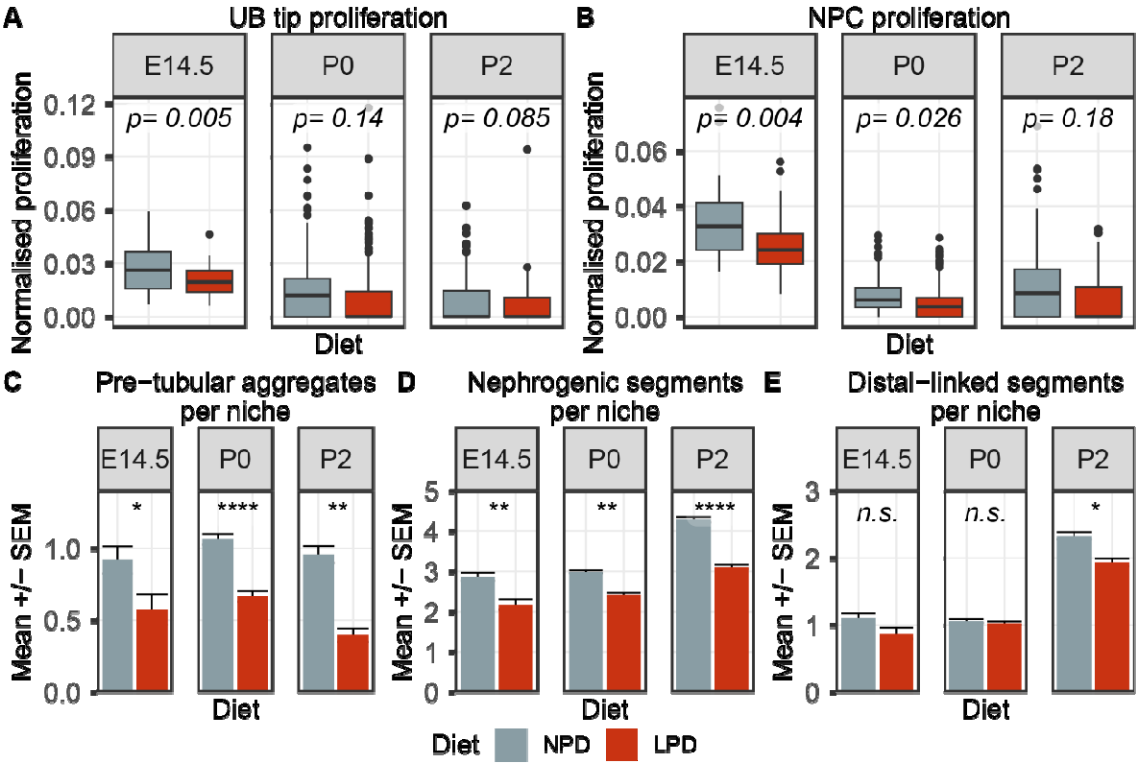

Figure 3.

Analysis of proliferation and early nascent nephrons at E14.5, P0 and P2. Proliferation of the ureteric bud tip in LPD offspring is reduced at E14.5 but is indifferent later in development (A), while NPC proliferation is impacted at E14.5 and P0 but not P2 towards the end of nephrogenesis (B). The number of pretubular aggregates (C) and total nephrogenic segments per niche are reduced throughout development in LPD offspring (D). While the number of distal-linked segments per niche appears to be indifferent at E14.5 and P0, they are reduced by P2 (E). Sample numbers, n = 38/40 niches (n = 4/4 kidneys) (NPD/LPD) at E14.5, n = 282/282 niches (9/11 kidneys) (NPD/LPD) at P0, n = 145/144 niches (n=7/7 kidneys) (NPD/LPD) at P2. *p < 0.05, **p < 0.01, ***p < 0.001, ****p < 0.0001, n.s. = not significant.

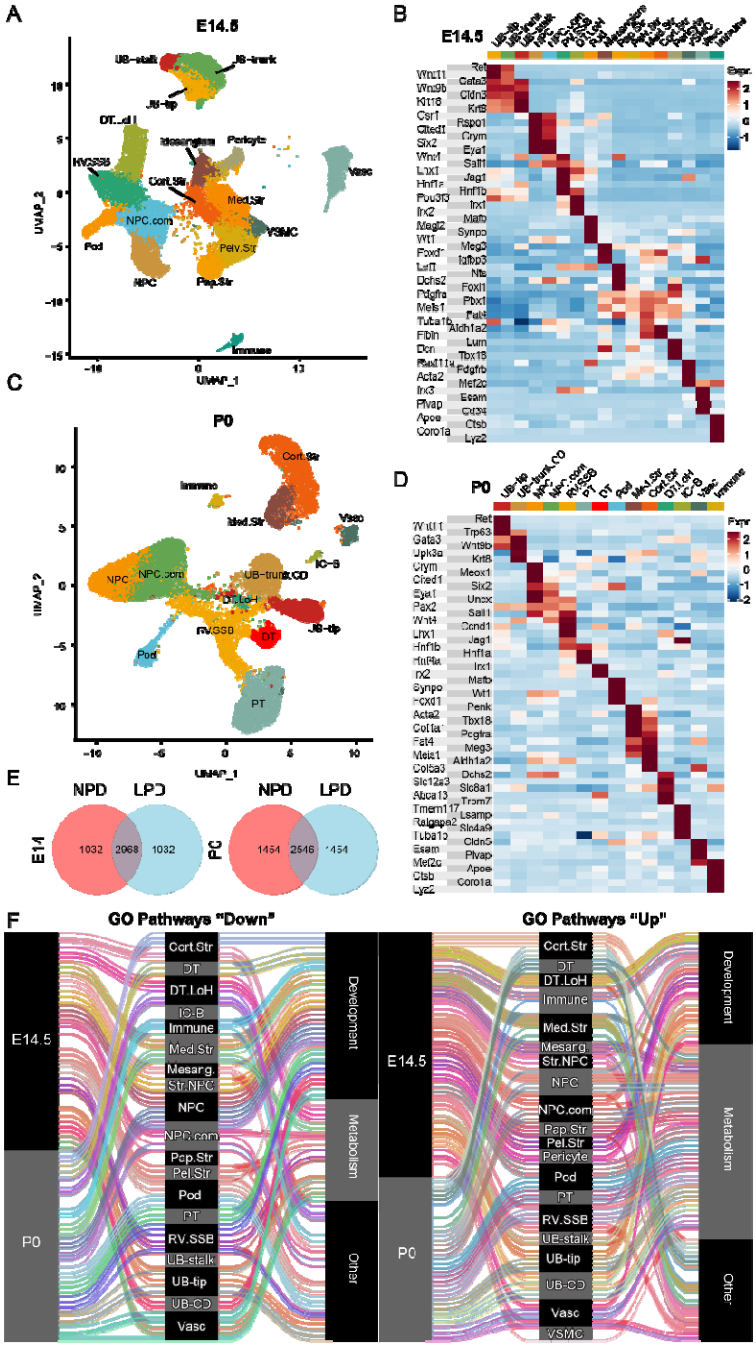

Figure 4.

Single-cell and nuclear analysis reveals overarching developmental and metabolic changes in gene expression. Viewed in UMAP reduced dimension space, clusters identified at E14.5 from single-cell sequencing (A) partition into known kidney cell types typified by canonical cell type markers (B), and likewise from P0 single nuclear sequencing (C), clusters represent known developmental cell types (D). Analyzing the most variable genes between NPD and LPD diets at both ages (E) a significant proportion of the most variable genes are unique to the diets. Assessing the top 3 associated ontologies of the differentially expressed genes in every cluster reveals an overarching developmental and metabolic effect on the kidney (F).

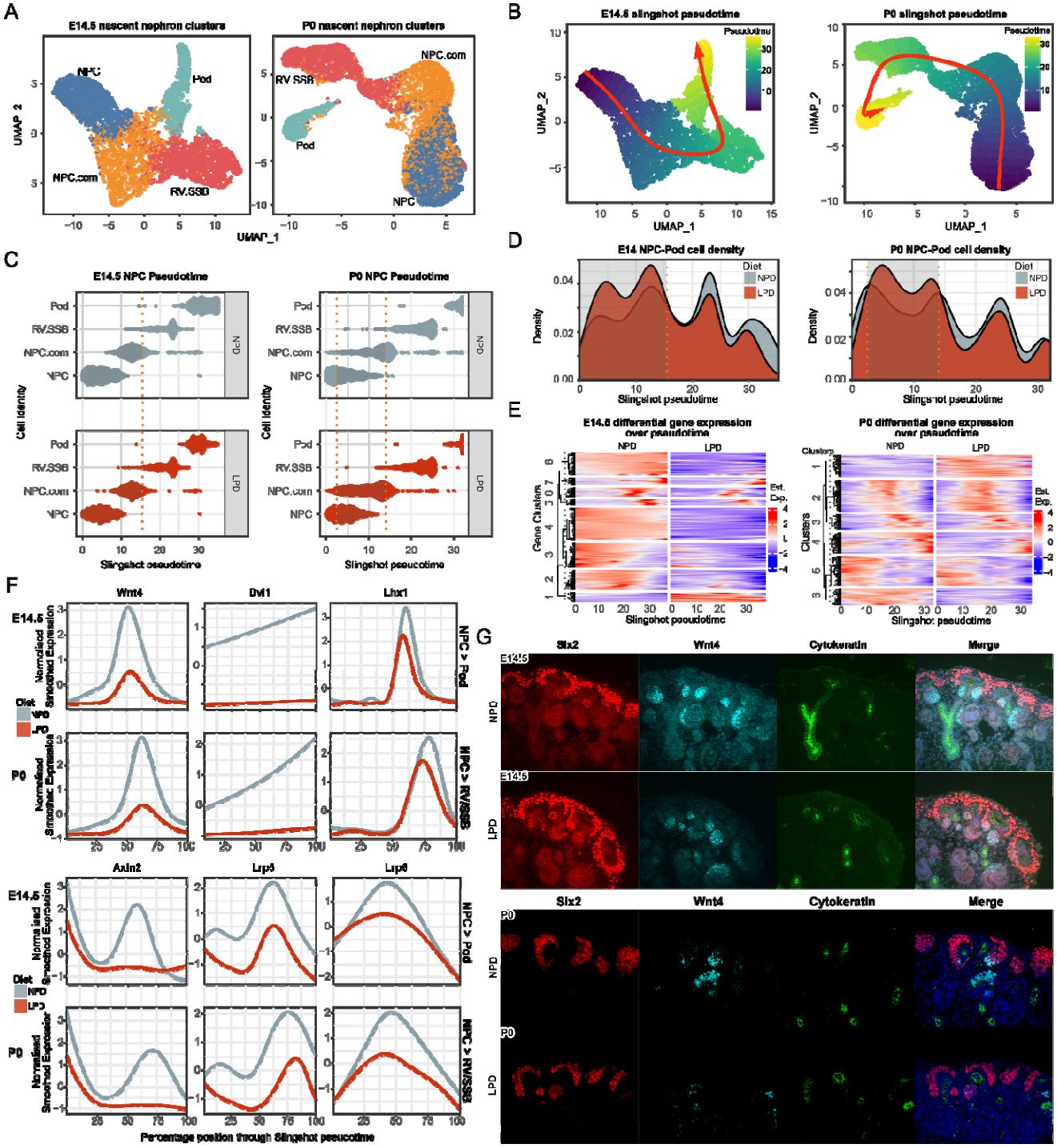

Figure 5.

Pseudotime trajectory analysis of the nephrogenic lineage indicates changes in cell development and nephrogenesis-promoting gene expression. NPC, committing NPC (NPC.com), renal vesicle – s-shaped body (RV/SSB) and Podocytes were subset from the whole

kidney dataset and reclustered (A). Slingshot was used to infer pseudotime (B), and the resulting timeline recapitulated known nephrogenic progression from NPC to Podocytes (C). The distribution of cells across pseudotime (D) shows a higher density of LPD cells weighted towards the beginning of pseudotime at both E14.5 and P0 (the orange-dotted grey zones, which are matched between ages in panels C, and D). Clustering of the dynamic changes in expression of the differentially expressed genes across pseudotime (E) indicates half of the clusters represent genes involved in cellular metabolic and nephrogenesis pathways. *Wnt* (F) and *Notch* genes important for nephrogenesis are generally downregulated over pseudotime (NPC to Podocyte at E14.5, and NPC to RV/SSB at P0). (G) Expression of WNT4 (cyan) in the developing nephrons is reduced in the E14.5 and P0, with nephron progenitor cells marked by SIX2 (red), ureteric tree by cytokeratin (green) and DNA (blue).

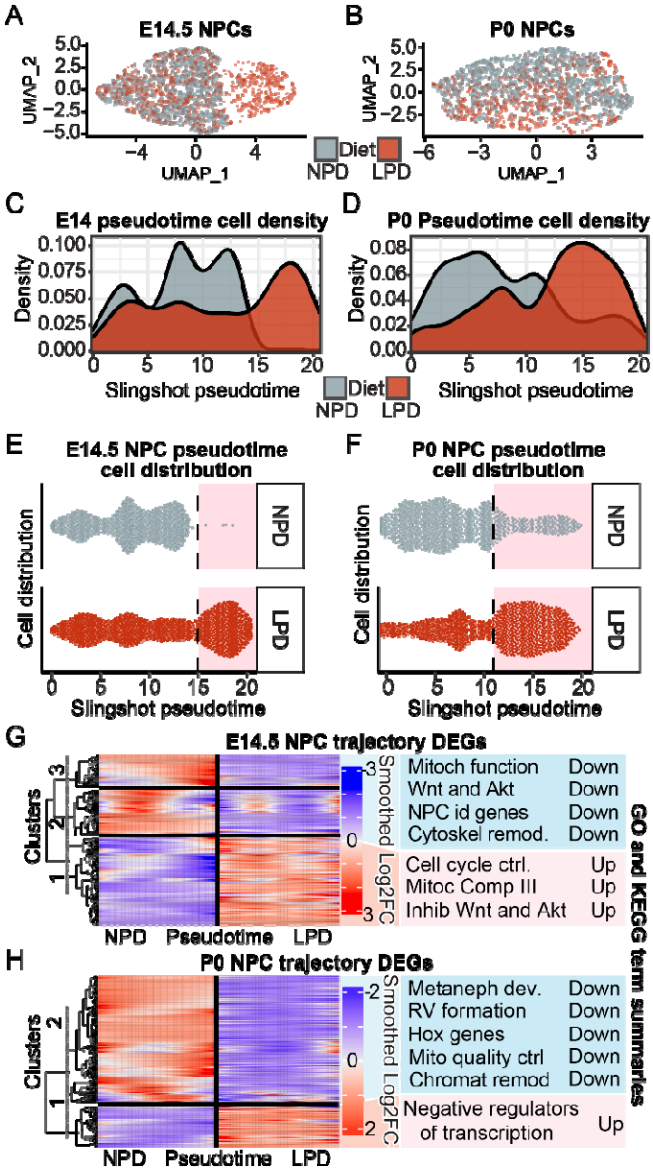

Figure 6.

The naïve nephron progenitor cell development and commitment is disrupted by LPD. Partitioning of the NPCs from the whole kidney dataset at E14.5 (A) and P0 (B), reveals diet-specific clusters in UMAP space. Pseudotime analysis shows a change in the differentiation state of cells at E14.5 and P0 (C, D), with a disruption in the distribution of cells (E, F). Cells more advanced in the pseudotime trajectory at E14.5 (G) are LPD specific, while at P0 (H) there is a greater abundance of cells at the beginning of pseudotime. Changes in gene expression across the trajectory indicate multiple pathways are up and downregulated which relate to cell differentiation, specification and cell cycle and mitochondrial function (G, H).

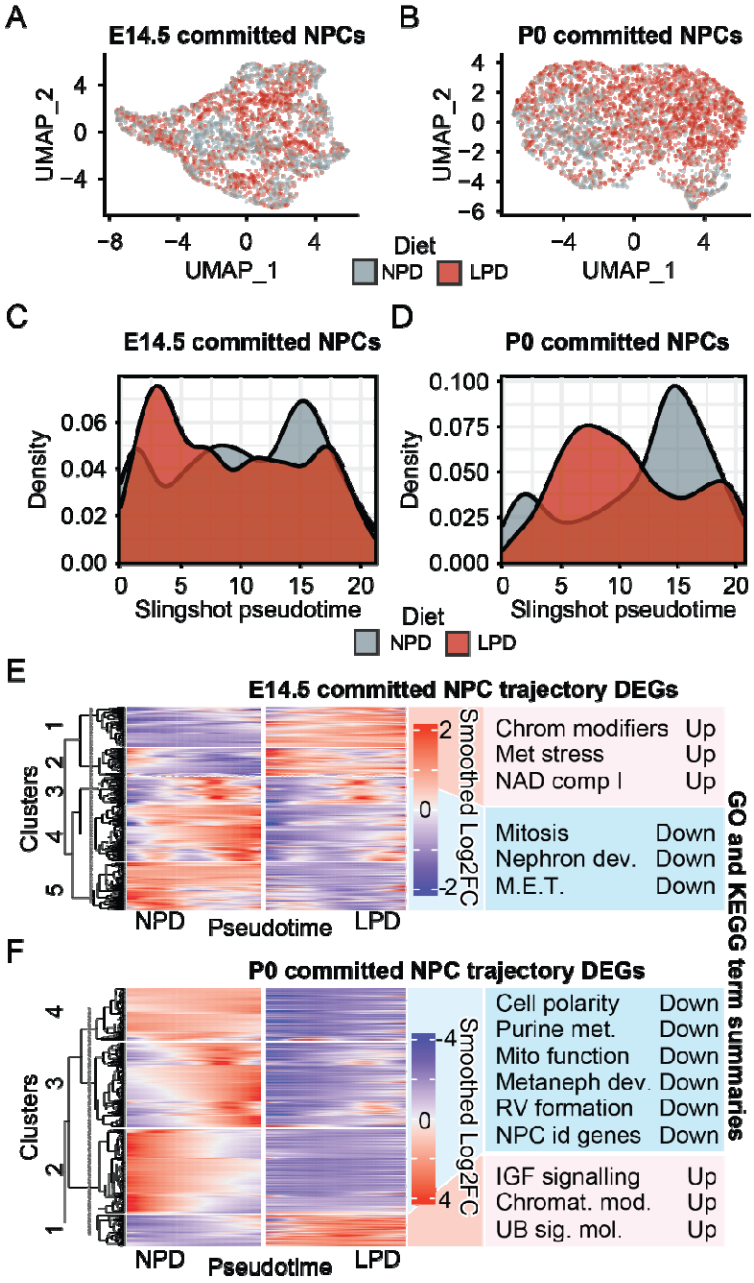

Figure 7.

Differentiation of committed NPCs is impeded by LPD. With committed nephron progenitor cells subclustered from the kidney datasets, there are areas of enrichment of NPD and LPD cells (A, B). The distribution of cells across pseudotime (C, D) mirrors that of the naïve nephron progenitors. The changes in gene expression across the pseudotime trajectory at E14.5 (E) and P0 (F) indicate nephron development, cell proliferation, metabolism and renal vesicle genes are misregulated.

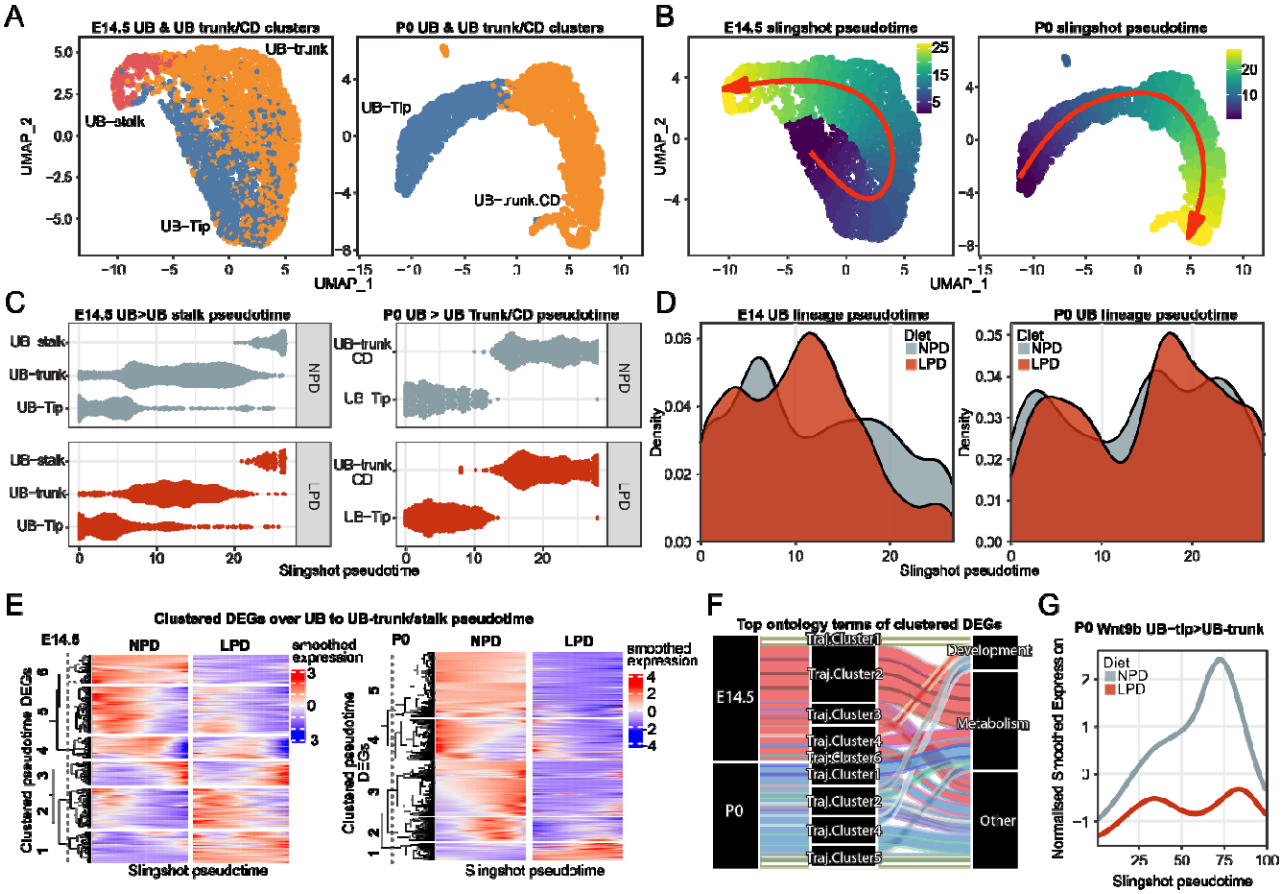

Figure 8.

Single-cell analysis of ureteric development at E14.5 and P0. The ureteric lineage from tip to stalk in early development (E14.5) and tip to trunk/collecting duct at P0 was subset from the entire single-cell dataset and re-clustered (A). Pseudotime trajectory analysis followed the established developmental progression of ureteric development (B, C). The distribution of cells indicates a greater proportion of LPD cells in the middle of pseudotime at the approximate point of trunk differentiation at E14.5 but not P0 (D). Analysis of differential gene expression across pseudotime (E) revealed many genes with similar expression profiles having altered expression. Wnt4, a renal vesicle specification gene was downregulated near the middle of pseudotime (F), and the other genes mostly clustered into metabolism pathways (G).

Gene	LogFC	LogCPM	PValue	Age	Direction
Hnrnpa0	-1.318	9.277	1.49E-84	E14	Down
Ybx3	**-1.090**	**9.351**	**8.79E-68**	**E14**	**Down**
Ptn	-0.884	9.201	6.82E-35	E14	Down
Rcc2	**-0.546**	**9.109**	**2.50E-15**	**E14**	**Down**
Ubb	-0.540	10.748	1.06E-61	E14	Down
Gpc3	**-0.525**	**9.417**	**7.92E-19**	**E14**	**Down**
Snhg12	0.552	9.060	5.38E-14	E14	Up
Tgfbl	**0.580**	**9.102**	**1.23E-15**	**E14**	**Up**
Erh	0.589	9.130	1.67E-17	E14	Up
Crym	**0.990**	**9.655**	**3.99E-65**	**E14**	**Up**
Glo1	1.178	9.389	1.12E-76	E14	Up
Aldh1a2	**1.284**	**9.000**	**7.46E-53**	**E14**	**Up**
Rbfox1	-0.950	12.154	2.14E-55	***P0***	Down
Lhfp	**-0.840**	**11.150**	**3.04E-23**	***P0***	**Down**
Cdh4	-0.821	11.245	3.39E-22	***P0***	Down
Dach1	**-0.769**	**11.188**	**1.39E-21**	***P0***	**Down**
Pdgfc	-0.744	11.482	7.81E-25	***P0***	Down
Mdga2	**-0.670**	**11.177**	**5.76E-14**	***P0***	**Down**
Strbp	0.422	11.213	2.80E-08	***P0***	Up
App	**0.427**	**11.269**	**9.03E-09**	***P0***	**Up**
Malat1	0.435	16.608	1.72E-47	***P0***	Up
Fgfr2	**0.444**	**11.221**	**4.68E-09**	***P0***	**Up**
Hdac8	0.523	11.345	5.44E-12	***P0***	Up
H3f3b	**0.568**	**11.212**	**1.42E-13**	***P0***	**Up**

Table 1.

E14.5 and P0 DEG between NPD and LPD NPC. The table presents the DEG between NPC from NPD and LPD cohort (cutoff log FC greater than |0.5| and p-value < 0.05). DEG list was generated with EdgeR as described in Methods. p-value threshold for the differences was set as p<0.05. logFC = log of the fold change difference; logCPM= log of counts per million reads mapped; PValue = calculated p-value for differences.

Gene	LogFC	LogCPM	PValue	Age	Direction
Hnrnpa0	-1.400	9.276	1.73E-125	E14	Down
Ybx3	**-0.940**	**9.309**	**2.62E-67**	**E14**	**Down**
Cdk2ap1	-0.813	9.016	2.97E-41	E14	Down
Rcc2	**-0.730**	**9.136**	**4.59E-39**	**E14**	**Down**
Wfdc2	-0.612	9.043	9.58E-17	E14	Down
Ccnd1	**-0.602**	**9.278**	**3.34E-15**	**E14**	**Down**
Erh	0.610	9.110	1.72E-25	E14	Up
Aldh1a2	**0.725**	**9.111**	**3.33E-27**	**E14**	**Up**
Hist1h2ae	0.870	9.032	1.74E-31	E14	Up
Crym	**1.020**	**9.241**	**1.52E-56**	**E14**	**Up**
Glo1	1.074	9.249	5.10E-79	E14	Up
Hist1h2ap	**1.609**	**9.404**	**1.53E-99**	**E14**	**Up**
Tenm4	-1.269	11.449	8.27E-62	***P0***	Down
Dach1	**-1.125**	**11.602**	**5.83E-57**	***P0***	**Down**
Pax2	-0.984	11.896	3.97E-52	***P0***	Down
Dab1	**-0.905**	**11.480**	**1.90E-32**	***P0***	**Down**
Bmper	-0.890	11.703	5.07E-33	***P0***	Down
Pdgfc	**-0.870**	**11.491**	**3.63E-32**	***P0***	**Down**
Rbm39	0.357	11.815	1.41E-07	***P0***	Up
Rev3l	**0.358**	**11.463**	**5.12E-06**	***P0***	**Up**
Malat1	0.369	16.936	1.57E-40	***P0***	Up
Hmcn1	**0.386**	**11.577**	**4.38E-07**	***P0***	**Up**
Klhdc10	0.399	11.435	1.84E-06	***P0***	Up
Epo	**0.802**	**11.390**	**6.50E-22**	***P0***	**Up**

Table 2.

E14.5 and P0 DEG between NPD and LPD NPC comm cluster. The table presents the DEG between NPC comm from NPD and LPD cohort (cutoff log FC greater than |0.5| and p-value < 0.05). DEG list was generated with EdgeR as described Methods. p-value threshold for the differences was set as p<0.05. logFC = log of the fold change difference; logCPM= log of counts per million reads mapped; PValue = calculated p-value for differences.

Gene	LogFC	LogCPM	PValue	Age	Direction
Hnrnpa0	-1.193	9.183	1.09E-41	E14	Down
Ybx3	**-0.992**	**9.002**	**7.21E-27**	**E14**	**Down**
H19	-0.703	9.025	1.80E-11	E14	Down
Rcc2	**-0.686**	**9.180**	**7.43E-20**	**E14**	**Down**
Gpc3	-0.685	9.192	1.55E-16	E14	Down
Cdk2ap1	**-0.676**	**8.940**	**3.96E-14**	**E14**	**Down**
Hoxb9	0.530	8.884	7.31E-08	E14	Up
Hist1h2ae	**0.645**	**9.130**	**5.76E-13**	**E14**	**Up**
Aldh1a3	0.957	9.075	2.89E-25	E14	Up
Btg2	**1.071**	**8.882**	**5.89E-27**	**E14**	**Up**
Glo1	1.187	9.341	2.00E-60	E14	Up
Hist1h2ap	**1.407**	**9.651**	**2.17E-68**	**E14**	**Up**
Hdac9	-0.972	11.559	7.01E-17	***P0***	Down
Erbb4	**-0.857**	**11.973**	**1.47E-16**	***P0***	**Down**
Nos1ap	-0.843	11.362	1.72E-12	***P0***	Down
Fgf12	**-0.821**	**11.286**	**1.32E-11**	***P0***	**Down**
Ctnnd2	-0.803	11.800	9.07E-14	***P0***	Down
Robo1	**-0.760**	**11.451**	**7.21E-11**	***P0***	**Down**
Rbm25	0.410	11.387	1.04E-03	***P0***	Up
Mbnl2	**0.455**	**11.290**	**3.97E-04**	***P0***	**Up**
Rbm39	0.464	11.678	8.10E-06	***P0***	Up
Strbp	**0.501**	**11.418**	**3.21E-05**	***P0***	**Up**
Esrrg	0.506	11.417	1.11E-04	***P0***	Up
H3f3b	**0.517**	**11.353**	**2.27E-05**	***P0***	**Up**

Table 3.

E14.5 and P0 DEG between NPD and LPD UB-tip clusters. The table presents the DEG between UB-tip from NPD and LPD cohort (cutoff log FC greater than |0.5| and p-value < 0.05). DEG list was generated with EdgeR as described in Methods. p-value threshold for the differences was set as p<0.05. logFC = log of the fold change difference; logCPM= log of counts per million reads mapped; PValue = calculated p-value for differences.

References

Ayres, J. A., L. Shum, A. N. Akarsu, R. Dashner, K. Takahashi, T. Ikura, H. C. Slavkin and G. H. Nuckolls (2001). "DACH: genomic characterization, evaluation as a candidate for postaxial polydactyly type A2, and developmental expression pattern of the mouse homologue." Genomics **77**(1-2): 18-26.

Bertram, J. F., R. N. Douglas-Denton, B. Diouf, M. D. Hughson and W. E. Hoy (2011). "Human nephron number: implications for health and disease." Pediatr Nephrol **26**(9): 1529-1533.

Brawley, L., S. Itoh, C. Torrens, A. Barker, C. Bertram, L. Poston and M. Hanson (2003). "Dietary protein restriction in pregnancy induces hypertension and vascular defects in rat male offspring." Pediatr Res **54**(1): 83-90.

Carroll, T. J., J. S. Park, S. Hayashi, A. Majumdar and A. P. McMahon (2005). "Wnt9b plays a central role in the regulation of mesenchymal to epithelial transitions underlying organogenesis of the mammalian urogenital system." Dev Cell **9**(2): 283-292.

Chevalier, R. L. (2020). "Bioenergetic Evolution Explains Prevalence of Low Nephron Number at Birth: Risk Factor for CKD." Kidney360 **1**(8): 863-879.

Combes, A. N., B. Phipson, K. T. Lawlor, A. Dorison, R. Patrick, L. Zappia, R. P. Harvey, A. Oshlack and M. H. Little (2019). "Single cell analysis of the developing mouse kidney provides deeper insight into marker gene expression and ligand-receptor crosstalk." Development **146**(12).

Combes, A. N., K. M. Short, J. Lefevre, N. A. Hamilton, M. H. Little and I. M. Smyth (2014). "An integrated pipeline for the multidimensional analysis of branching morphogenesis." Nat Protoc **9**(12): 2859-2879.

Cooke, A., T. Schwarzl, I. Huppertz, G. Kramer, P. Mantas, A. M. Alleaume, W. Huber, J. Krijgsveld and M. W. Hentze (2019). "The RNA-Binding Protein YBX3 Controls Amino Acid Levels by Regulating SLC mRNA Abundance." Cell Rep **27**(11): 3097-3106 e3095.

Cullen-McEwen, L. A., J. A. Armitage, J. R. Nyengaard and J. F. Bertram (2012). "Estimating nephron number in the developing kidney using the physical disector/fractionator combination." Methods Mol Biol **886**: 109-119.

de Onis, M., C. Monteiro, J. Akre and G. Glugston (1993). "The worldwide magnitude of protein-energy malnutrition: an overview from the WHO Global Database on Child Growth." Bull World Health Organ **71**(6): 703-712.

Diaz-Cuadros, M., T. P. Miettinen, O. S. Skinner, D. Sheedy, C. M. Diaz-Garcia, S. Gapon, A. Hubaud, G. Yellen, S. R. Manalis, W. M. Oldham and O. Pourquie (2023). "Metabolic regulation of species-specific developmental rates." Nature **616**(7956): E4.

Ding, H., X. Wu, I. Kim, P. P. Tam, G. Y. Koh and A. Nagy (2000). "The mouse Pdgfc gene: dynamic expression in embryonic tissues during organogenesis." Mech Dev **96**(2): 209-213.

Fernandes-Silva, H., M. G. Alves, H. Araujo-Silva, A. M. Silva, J. Correia-Pinto, P. F. Oliveira and R. S. Moura (2021). "Lung branching morphogenesis is accompanied by temporal metabolic changes towards a glycolytic preference." Cell Biosci **11**(1): 134.

Ghosh, S., D. Suri and R. Uauy (2012). "Assessment of protein adequacy in developing countries: quality matters." Br J Nutr **108 Suppl 2**: S77-87.

Goyal, R. and L. D. Longo (2013). "Maternal protein deprivation: sexually dimorphic programming of hypertension in the mouse." Hypertens Res **36**(1): 29-35.

Grote, S. (2023). GOfuncR: Gene ontology enrichment using FUNC.

Grubman, A., G. Chew, J. F. Ouyang, G. Sun, X. Y. Choo, C. McLean, R. K. Simmons, S. Buckberry, D. B. Vargas-Landin, D. Poppe, J. Pflueger, R. Lister, O. J. L. Rackham, E. Petretto and J. M. Polo

(2019). "A single-cell atlas of entorhinal cortex from individuals with Alzheimer's disease reveals cell-type-specific gene expression regulation." Nat Neurosci **22**(12): 2087-2097.
Guo, Q., A. Kim, B. Li, A. Ransick, H. Bugacov, X. Chen, N. Lindstrom, A. Brown, L. Oxburgh, B. Ren and A. P. McMahon (2021). "A beta-catenin-driven switch in TCF/LEF transcription factor binding to DNA target sites promotes commitment of mammalian nephron progenitor cells." Elife **10**.
Hadley Wickham, M. A., Jennifer Bryan, Winston Chang, Lucy D'Agostino McGowan, Romain François, Garrett Grolemund, Alex Hayes, Lionel Henry, Jim Hester, Max Kuhn, Thomas Lin Pedersen, Evan Miller, Stephan Milton Bache, Kirill Müller, Jeroen Ooms, David Robinson, Dana Paige Seidel, Vitalie Spinu, Kohske Takahashi, Davis Vaughan, Claus Wilke, Kara Woo, Hiroaki Yutani (2019). "Welcome to the Tidyverse." Journal of Open Source Software **4**(43): 6.
Hao, Y., S. Hao, E. Andersen-Nissen, W. M. Mauck, 3rd, S. Zheng, A. Butler, M. J. Lee, A. J. Wilk, C. Darby, M. Zager, P. Hoffman, M. Stoeckius, E. Papalexi, E. P. Mimitou, J. Jain, A. Srivastava, T. Stuart, L. M. Fleming, B. Yeung, A. J. Rogers, J. M. McElrath, C. A. Blish, R. Gottardo, P. Smibert and R. Satija (2021). "Integrated analysis of multimodal single-cell data." Cell **184**(13): 3573-3587 e3529.
Hoppe, C. C., R. G. Evans, K. M. Moritz, L. A. Cullen-McEwen, S. M. Fitzgerald, J. Dowling and J. F. Bertram (2007). "Combined prenatal and postnatal protein restriction influences adult kidney structure, function, and arterial pressure." Am J Physiol Regul Integr Comp Physiol **292**(1): R462-469.
Huang, D. W., B. T. Sherman, Q. Tan, J. Kir, D. Liu, D. Bryant, Y. Guo, R. Stephens, M. W. Baseler, H. C. Lane and R. A. Lempicki (2007). "DAVID Bioinformatics Resources: expanded annotation database and novel algorithms to better extract biology from large gene lists." Nucleic Acids Res **35**(Web Server issue): W169-175.
Ikeda, K., Y. Watanabe, H. Ohto and K. Kawakami (2002). "Molecular interaction and synergistic activation of a promoter by Six, Eya, and Dach proteins mediated through CREB binding protein." Mol Cell Biol **22**(19): 6759-6766.
Kakaei, H., H. Nourmoradi, S. Bakhtiyari, M. Jalilian and A. Mirzaei (2022). "Effect of COVID-19 on food security, hunger, and food crisis." COVID-19 and the Sustainable Development Goals: 3-29.
Karner, C. M., R. Chirumamilla, S. Aoki, P. Igarashi, J. B. Wallingford and T. J. Carroll (2009). "Wnt9b signaling regulates planar cell polarity and kidney tubule morphogenesis." Nat Genet **41**(7): 793-799.
Karner, C. M., A. Das, Z. Ma, M. Self, C. Chen, L. Lum, G. Oliver and T. J. Carroll (2011). "Canonical Wnt9b signaling balances progenitor cell expansion and differentiation during kidney development." Development **138**(7): 1247-1257.
Kim, J. Y., J. H. Jung, S. J. Lee, S. S. Han and S. H. Hong (2022). "Glyoxalase 1 as a Therapeutic Target in Cancer and Cancer Stem Cells." Mol Cells **45**(12): 869-876.
Kispert, A., S. Vainio and A. P. McMahon (1998). "Wnt-4 is a mesenchymal signal for epithelial transformation of metanephric mesenchyme in the developing kidney." Development **125**(21): 4225-4234.
Langley-Evans, S. C., S. J. Welham and A. A. Jackson (1999). "Fetal exposure to a maternal low protein diet impairs nephrogenesis and promotes hypertension in the rat." Life Sci **64**(11): 965-974.
Lefevre, J. G., K. M. Short, T. O. Lamberton, O. Michos, D. Graf, I. M. Smyth and N. A. Hamilton (2017). "Branching morphogenesis in the developing kidney is governed by rules that pattern the ureteric tree." Development **144**(23): 4377-4385.

Li, X., A. Ponten, K. Aase, L. Karlsson, A. Abramsson, M. Uutela, G. Backstrom, M. Hellstrom, H. Bostrom, H. Li, P. Soriano, C. Betsholtz, C. H. Heldin, K. Alitalo, A. Ostman and U. Eriksson (2000). "PDGF-C is a new protease-activated ligand for the PDGF alpha-receptor." Nat Cell Biol **2**(5): 302-309.

Li, Y., J. Liu, W. Li, A. Brown, M. Baddoo, M. Li, T. Carroll, L. Oxburgh, Y. Feng and Z. Saifudeen (2015). "p53 Enables metabolic fitness and self-renewal of nephron progenitor cells." Development **142**(7): 1228-1241.

Liu, J., F. Edgington-Giordano, C. Dugas, A. Abrams, P. Katakam, R. Satou and Z. Saifudeen (2017). "Regulation of Nephron Progenitor Cell Self-Renewal by Intermediary Metabolism." J Am Soc Nephrol **28**(11): 3323-3335.

Luo, Y., K. Dallaglio, Y. Chen, W. A. Robinson, S. E. Robinson, M. D. McCarter, J. Wang, R. Gonzalez, D. C. Thompson, D. A. Norris, D. R. Roop, V. Vasiliou and M. Fujita (2012). "ALDH1A isozymes are markers of human melanoma stem cells and potential therapeutic targets." Stem Cells **30**(10): 2100-2113.

Luyckx, V. A. and B. M. Brenner (2010). "The clinical importance of nephron mass." J Am Soc Nephrol **21**(6): 898-910.

Luyckx, V. A., K. Shukha and B. M. Brenner (2011). "Low nephron number and its clinical consequences." Rambam Maimonides Med J **2**(4): e0061.

Makayes, Y., E. Resnick, L. Hinden, E. Aizenshtein, T. Shlomi, R. Kopan, M. Nechama and O. Volovelsky (2021). "Increasing mTORC1 Pathway Activity or Methionine Supplementation during Pregnancy Reverses the Negative Effect of Maternal Malnutrition on the Developing Kidney." J Am Soc Nephrol.

McGrane, M. M., J. de Vente, J. Yun, J. Bloom, E. Park, A. Wynshaw-Boris, T. Wagner, F. M. Rottman and R. W. Hanson (1988). "Tissue-specific expression and dietary regulation of a chimeric phosphoenolpyruvate carboxykinase/bovine growth hormone gene in transgenic mice." J Biol Chem **263**(23): 11443-11451.

Merlet-Benichou, C., T. Gilbert, M. Muffat-Joly, M. Lelievre-Pegorier and B. Leroy (1994). "Intrauterine growth retardation leads to a permanent nephron deficit in the rat." Pediatr Nephrol **8**(2): 175-180.

Murawski, I. J., R. W. Maina and I. R. Gupta (2010). "The relationship between nephron number, kidney size and body weight in two inbred mouse strains." Organogenesis **6**(3): 189-194.

Nishimura, T. and M. Takeichi (2008). "Shroom3-mediated recruitment of Rho kinases to the apical cell junctions regulates epithelial and neuroepithelial planar remodeling." Development **135**(8): 1493-1502.

O'Brien, L. L. (2019). "Nephron progenitor cell commitment: Striking the right balance." Semin Cell Dev Biol **91**: 94-103.

Poladia, D. P., K. Kish, B. Kutay, J. Bauer, M. Baum and C. M. Bates (2006). "Link between reduced nephron number and hypertension: studies in a mutant mouse model." Pediatr Res **59**(4 Pt 1): 489-493.

Ritchie, M. E., B. Phipson, D. Wu, Y. Hu, C. W. Law, W. Shi and G. K. Smyth (2015). "limma powers differential expression analyses for RNA-sequencing and microarray studies." Nucleic Acids Res **43**(7): e47.

Sajithlal, G., D. Zou, D. Silvius and P. X. Xu (2005). "Eya 1 acts as a critical regulator for specifying the metanephric mesenchyme." Dev Biol **284**(2): 323-336.

Sakurai, H., K. T. Bush and S. K. Nigam (2001). "Identification of pleiotrophin as a mesenchymal factor involved in ureteric bud branching morphogenesis." Development **128**(17): 3283-3293.

Semba, R. D. (2016). "The Rise and Fall of Protein Malnutrition in Global Health." Ann Nutr Metab **69**(2): 79-88.
Sene, L. B., W. R. Scarano, A. Zapparoli, J. A. R. Gontijo and P. A. Boer (2021). "Impact of gestational low-protein intake on embryonic kidney microRNA expression and in nephron progenitor cells of the male fetus." PLoS One **16**(2): e0246289.
Short, K., M. Hodson and I. Smyth (2013). "Spatial mapping and quantification of developmental branching morphogenesis." Development **140**(2): 471-478.
Short, K. M., A. N. Combes, J. Lefevre, A. L. Ju, K. M. Georgas, T. Lamberton, O. Cairncross, B. A. Rumballe, A. P. McMahon, N. A. Hamilton, I. M. Smyth and M. H. Little (2014). "Global quantification of tissue dynamics in the developing mouse kidney." Dev Cell **29**(2): 188-202.
Short, K. M., A. N. Combes, V. Lisnyak, J. G. Lefevre, L. K. Jones, M. H. Little, N. A. Hamilton and I. M. Smyth (2018). "Branching morphogenesis in the developing kidney is not impacted by nephron formation or integration." Elife **7**.
Short, K. M., M. J. Hodson and I. M. Smyth (2010). "Tomographic quantification of branching morphogenesis and renal development." Kidney Int **77**(12): 1132-1139.
Sima, J., B. Zhang, X. Y. Sima and Y. X. Mao (2016). "Overexpression of BTG2 suppresses growth, migration, and invasion of human renal carcinoma cells in vitro." Neoplasma **63**(3): 385-393.
Street, K., D. Risso, R. B. Fletcher, D. Das, J. Ngai, N. Yosef, E. Purdom and S. Dudoit (2018). "Slingshot: cell lineage and pseudotime inference for single-cell transcriptomics." BMC Genomics **19**(1): 477.
Thibault, P. A., A. Ganesan, S. Kalyaanamoorthy, J. W. E. Clarke, H. E. Salapa and M. C. Levin (2021). "hnRNP A/B Proteins: An Encyclopedic Assessment of Their Roles in Homeostasis and Disease." Biology (Basel) **10**(8).
Torrence, M. E., M. R. MacArthur, A. M. Hosios, A. J. Valvezan, J. M. Asara, J. R. Mitchell and B. D. Manning (2021). "The mTORC1-mediated activation of ATF4 promotes protein and glutathione synthesis downstream of growth signals." Elife **10**.
Van den Berge, K., H. Roux de Bezieux, K. Street, W. Saelens, R. Cannoodt, Y. Saeys, S. Dudoit and L. Clement (2020). "Trajectory-based differential expression analysis for single-cell sequencing data." Nat Commun **11**(1): 1201.
Veikkolainen, V., F. Naillat, A. Railo, L. Chi, A. Manninen, P. Hohenstein, N. Hastie, S. Vainio and K. Elenius (2012). "ErbB4 modulates tubular cell polarity and lumen diameter during kidney development." J Am Soc Nephrol **23**(1): 112-122.
Wanek, N., K. Muneoka, G. Holler-Dinsmore, R. Burton and S. V. Bryant (1989). "A staging system for mouse limb development." J Exp Zool **249**(1): 41-49.
Woods, L. L., J. R. Ingelfinger, J. R. Nyengaard and R. Rasch (2001). "Maternal protein restriction suppresses the newborn renin-angiotensin system and programs adult hypertension in rats." Pediatr Res **49**(4): 460-467.
Woods, L. L., D. A. Weeks and R. Rasch (2004). "Programming of adult blood pressure by maternal protein restriction: role of nephrogenesis." Kidney Int **65**(4): 1339-1348.
Wu, X., W. Liu and H. Ding (2018). "A Pdgf-c(CreERT2) knock-in mouse model for tracing PDGF-C cell lineages during development." Genesis **56**(2).
Zeman, F. J. (1968). "Effects of maternal protein restriction on the kidney of the newborn young of rats." J Nutr **94**(2): 111-116.

Supplementary Data S1 - Raw data will be made available with the final version.

Supplementary Data S2 - Raw data will be made available with the final version.